

Geophysical Research Letters

RESEARCH LETTER

10.1002/2017GL076761

Key Points:

- The width of the locked region decreases stepwise from NE to SW along strike
- Three sharp boundaries that mark changes in fault coupling are identified
- The change in preexisting fabric orientation contributes significantly to the change in fault locking and subduction seismicity

Supporting Information:

- Supporting Information S1
- Table S1
- Table S2
- Movie S1
- Movie S2
- Movie S3
- Movie S4
- Movie S5
- Movie S6

Correspondence to:

S. Li,
sli11@alaska.edu

Citation:

Li, S., & Freymueller, J. T. (2018). Spatial variation of slip behavior beneath the Alaska Peninsula along Alaska-Aleutian subduction zone. *Geophysical Research Letters*, 45, 3453–3460. <https://doi.org/10.1002/2017GL076761>

Received 18 DEC 2017

Accepted 28 MAR 2018

Accepted article online 2 APR 2018

Published online 21 APR 2018

©2018. American Geophysical Union.
All Rights Reserved.

Spatial Variation of Slip Behavior Beneath the Alaska Peninsula Along Alaska-Aleutian Subduction Zone

Shanshan Li¹  and Jeffrey T. Freymueller¹ 

¹Geophysical Institute, University of Alaska Fairbanks, Fairbanks, AK, USA

Abstract We resurveyed preexisting campaign Global Positioning System (GPS) sites and estimated a highly precise GPS velocity field for the Alaska Peninsula. We use the TDEFNODE software to model the slip deficit distribution using the new GPS velocities. We find systematic misfits to the vertical velocities from the optimal model that fits the horizontal velocities well, which cannot be explained by altering the slip distribution, so we use only the horizontal velocities in the study. Locations of three boundaries that mark significant along-strike change in the locking distribution are identified. The Kodiak segment is strongly locked, the Semidi segment is intermediate, the Shumagin segment is weakly locked, and the Sanak segment is dominantly creeping. We suggest that a change in preexisting plate fabric orientation on the downgoing plate has an important control on the along-strike variation in the megathrust locking distribution and subduction seismicity.

Plain Language Summary Understanding controls on slip behavior is a key objective of scientists from many different disciplines across solid earth sciences. Measuring the spatial changes in slip on the subduction plate interface can improve our understanding of factors that govern the size, location, and frequency of great destructive earthquakes. Does slip change abruptly or gradually along the length of the subduction zone? We estimate a new model that represents more precisely changes in slip on the interface between North American plate and Pacific plate beneath the Alaska Peninsula. We show that these changes in slip are abrupt and the locations of the changes correlate with features on the downgoing oceanic plate. The orientation of preexisting weakness on the Pacific plate correlates with the estimated slip variations and changes in the seismicity. In the areas that dominantly creep, the Pacific plate has been faulted extensively as it was bent going over the outer rise, leading to a rougher fault surface and more water being brought down with the subducted plate. In the areas that are mostly locked by friction, the faults in the Pacific plate are oriented nearly perpendicular to the trench and there is minimal faulting at the outer rise.

1. Introduction and Background

Subduction zones exhibit remarkable along-strike variations in seismic activity and in plate interface slip deficit worldwide. Understanding the cause of along-strike variations in slip behavior on the plate interface and seismic potential is important for better understanding the dynamic mechanical properties of the faults, and the rheology of the lower crust and lithosphere. Geodetic measurements can be used to study the process of the strain accumulation and estimate the extent of plate interface frictional locking or moment deficit on the plate interface. The Alaska Peninsula, which includes the Shumagin and Semidi segments of the Aleutian subduction zone, features a dramatic along-strike transition from a widely locked region to a mainly creeping area on the plate interface (Fournier & Freymueller, 2007).

A magnitude 8.3 earthquake in 1938 last ruptured the subduction interface from west of Kodiak Island to east of the Shumagin segment (Johnson & Satake, 1994). Fournier and Freymueller (2007) estimated that the plate interface is almost fully locked (70–90%) within the 1938 earthquake rupture zone (Figure 1a). The region between the 1946 earthquake (M_s 7.4) rupture zone and the 1938 earthquake (M_w 8.3) rupture zone was identified as a possible seismic gap in the 1970s (McCann et al., 1979). The eastern part of this region has a ~30% slip deficit, which is much smaller than the adjacent area within 1938 rupture zone, while the western part appears to be creeping at all depths (Fournier & Freymueller, 2007).

Marine seismic imaging studies in our study area document significant along-strike variations in the structure of the incoming plate that appear to be associated with changes in plate boundary behavior. Changes in the

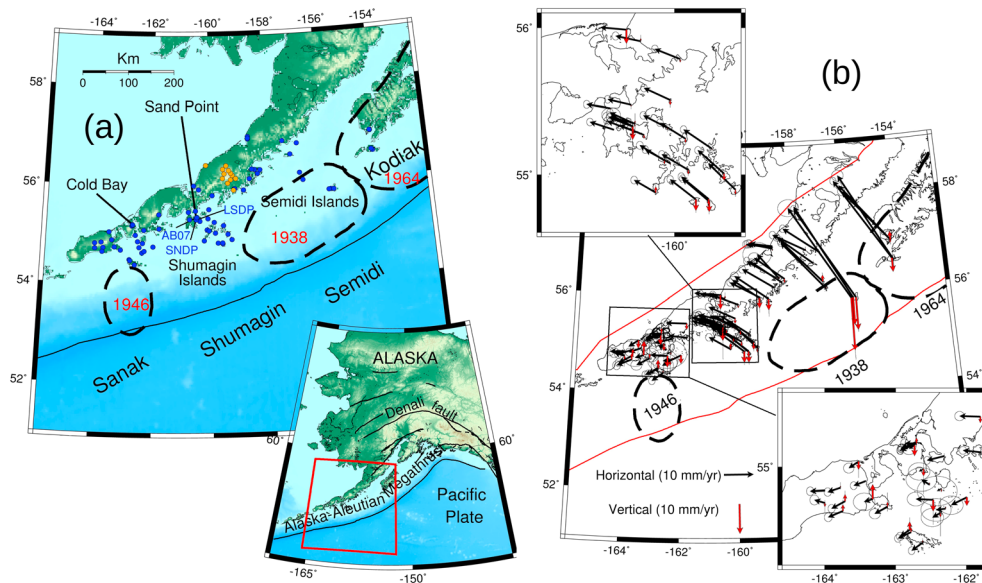


Figure 1. (a) Topographic map and tectonic setting (inset) of the study area on the Alaska Peninsula (red rectangle in inset map). Black dashed outlines show the rupture zone of past large earthquakes (Davies et al., 1981). Major towns are marked. The Alaska Peninsula are divided into four segments: Sanak, Shumagin, Semidi, and Kodiak. Blue dots are GPS stations used in this study. Orange dots are Global Positioning System (GPS) stations with significant volcano deformation. (b) Observed GPS velocities in horizontal (black) and vertical (red) for stations in the Alaska Peninsula.

amount of bending faulting and sediment thickness on the incoming plate have been proposed to contribute to a more heterogeneous megathrust in the Shumagin Gap than in the Semidi segment, which could have consequences for plate boundary behavior (Bécel et al., 2017; Shillington et al., 2015).

Our main goal for this study is to characterize the slip deficit along this segment of the Aleutian subduction zone and relate this to potential causes for the change in behavior. We inverted for the slip deficit distribution from a new dense Global Positioning System (GPS) velocity field (Figure 1b). Then we identified the locations of the along-strike boundaries that mark the transition from strongly to weakly locked segments of the subduction margin and explored their along-strike widths. We then correlate them with along-strike changes in preexisting fabric on the downgoing plate, and subduction seismicity.

2. Data

We used three component GPS velocities from 78 sites along the Alaska Peninsula, surveyed between 1992 and 2016 (Figure 1b and Table S2 in the supporting information) including both continuous and campaign stations. Subsets of the data were used earlier by Freymueller and Beavan (1999), Fletcher et al. (2001), and Fournier and Freymueller (2007, 2008). New observations of 35 campaign sites were made within the Shumagins and the 1938 rupture zone to the northeast in May–June 2016. These sites all had past measurements from up to 20 years ago, but many had been surveyed only once. With the long time span and additional measurements, we have a much denser site network than previous studies, with much lower uncertainties than the earlier GPS data sets. GPS sites located close to Veniaminof volcano have a large effect from volcano deformation (Fournier & Freymueller, 2008) and thus were not used (Figure 1a, orange dots).

We used the GIPSY/OASIS goa-5.0 software developed by Jet Propulsion Laboratory to obtain daily coordinate and covariance estimates for all the used continuous and campaign GPS stations in the Alaska Peninsula using point positioning. The GPS data analysis method was the same as Li et al. (2016). We adopted the Jet Propulsion Laboratory nonfiducial orbits and clock products and estimated a daily transformation for each daily solution into the ITRF2008 reference frame (Altamimi et al., 2011). We calculated velocities from the time series of each individual station by weighted least squares using all data within the survey period (1992–2016). We removed the GRACE-derived seasonal variation in the velocity fit (Zou et al., 2014) and estimated residual seasonal terms for the continuous sites. We also removed the geocenter translation rate error in ITRF2008 estimated by Argus et al. (2010) and rotated the velocities into a North America fixed

reference frame. We also removed models for Glacial Isostatic Adjustment (Hu & Freymueller, 2012) and 1964 postseismic deformation (Suito & Freymueller, 2009) from all GPS velocities. Both of these corrections have only a small effect within the study area.

The GPS velocity field (Figure 1b) reveals that the horizontal velocities are largest near the trench and decrease with distance from the trench due to elastic deformation from the locked subduction zone. There are also strong along-strike variations in the GPS horizontal velocities. Sites that are further east have larger velocities than those in the west, given the same distance from the trench. Sites in the west, especially within the Sanak segment, move in a nearly trench-parallel direction and show no variation in velocities with distance from the trench. The vertical velocities indicate that subsidence occurs in the eastern part of the Semidi segment and in the Shumagin segment. Some sites in the Semidi segment and Sanak segment show subsidence and others show uplift.

3. Method

In general, all the continuous GPS sites and all campaign sites with multiple surveys show linear motion with a constant site velocity, with the exception of one small slow slip event (Text S1, Figure S1, and Table S1). We found evidence for only minimal time variations in the slip distribution in the study region, so we assume that a constant velocity model describes all of the sites with only two surveys. We used TDEFNODE (McCaffrey, 2002) software to estimate the slip deficit rate distribution on the megathrust by inverting the GPS velocity data. We used Slab1.0 plate geometry (Hayes et al., 2012) to construct the slab interface. The slab was digitized about every 25 km in the along-strike direction and every 5 km in the downdip direction. We grouped together pairs of adjacent fault geometry nodes to have the same locking fraction, so the final grid of model parameters had 18 nodes in the along-strike direction and 7 nodes in the downdip direction, an average spacing of 50 and 10 km, respectively.

The entire upper plate in the Alaska Peninsula moves relative to North America (Cross & Freymueller, 2008; Freymueller et al., 2008), and we must account for this motion via a block model to avoid biasing the estimated slip distribution on the megathrust (Li et al., 2016). The block model uses the Southern Alaska block (SOAK) from Fletcher (2002), the Bering plate (BRNG) from Cross and Freymueller (2008), the Peninsula block (PENN) modified from Li et al. (2016), and two major plates: NOAM and PCFC (Sella et al., 2007; Text S2 and Figure S2). The estimated angular velocity of the PENN block in Li et al. (2016) used data from Cook Inlet and Alaska Peninsula; Cook Inlet appears to be moving slightly faster (~ 1 mm/year) than the Alaska Peninsula, leading to systematic trench-parallel residual in the GPS velocities here. So we reestimated the angular velocity of the PENN block using the sites within the Alaska Peninsula and sites in the eastern Aleutians as far west as Atka that show no strain from a locked megathrust and excluding sites from Cook Inlet (Text S2). The estimation of block rotation for PENN block used a different set of sites (Table S3) from those used in Li et al. (2016), selected to minimize potential biases from the locking model. After the estimation of the PENN block, we fixed all the block motions per Table S4 for the remaining inversions in this paper.

TDEFNODE combines spherical block rotations with interseismic fault locking distributions modeled as dislocations in an elastic half-space (Okada, 1985). Interseismic locking describes the slip deficit rate distribution on the megathrust. The plate interface is represented by a grid of nodes, and the locking fraction ϕ (ratio of the slip deficit rate to the long-term slip rate) is estimated at each node on a continuous fault geometry. In all the inversion models, we restricted the locking ratio ϕ to the range $[0, 1]$ where the brackets indicate minimum and maximum allowed locking values. Spatial smoothing in the along-strike and downdip directions was applied in the estimation of locking distribution.

4. Results

We first estimated the locking distribution on the plate interface beneath the Alaska Peninsula using three component GPS velocities. In this inversion model, we applied Laplacian smoothing with the same smoothing factors in both along-strike and downdip directions. Varying the smoothing factors generates a series of solutions where the curvature of the locking pattern is damped to varying degrees (e.g., Li et al., 2016). After analyzing the trade-off curve, we find that the optimal smoothing factors are $2 \cdot 10^8$ using both horizontal and vertical velocities (Figure S3) and $1 \cdot 10^8$ using horizontal velocities only (Figure S4). In the abovementioned model, there are long-wavelength systematic misfits to the vertical velocities while the model fits the

horizontal velocities fairly well. The vertical misfits cannot be explained by altering the slip distribution on the plate interface. Possible explanations for the systematic misfit are investigated in the supporting information (Text S3, DeGrandpre, 2015). Because the vertical velocities appear to contain a significant component in addition to the subduction zone deformation, we only used the horizontal velocities for the remainder of this study.

4.1. Slip Model for Subsegments

We found that a standard inversion model significantly oversmooths the locking distribution and underestimates the strong locking variations in along strike. In this inversion model, the area west of the Shumagin segment is barely affected by subduction strain, so high smoothing does not affect the slip distribution in this region (the best fitting slip deficit is nearly zero). However, the eastern part of the Alaska Peninsula has large variation of locking values, so high smoothing will smooth out the strong along-strike variation in the locking distribution and cause large data misfit.

From this smoothed inversion model, we can easily identify four different patterns in the locking distribution. Therefore, we divided the plate interface into four segments based on the observed along-strike variation from strongly locked in the northeast to mostly creeping in the southwest. We estimated the optimal smoothing factor and got the best fitting locking distribution for each segment individually (Figure S6). Then we averaged the locking values along strike for each segment and combined all the segments to generate an initial locking distribution on the slab interface beneath the Alaska Peninsula. With this locking distribution, we constructed a forward model (Figure S7) with a smaller data residual than the smoothed inversion model (comparable to extremely rough models that contain obvious artifacts, see Text S4 and Figures S4 and S5). The improvement in data fit comes from having sharp along-strike boundaries, while strong along-strike smoothing within each segment does not degrade model fit.

4.2. Locating the Boundaries That Mark Sharp Changes in Locking

Given the optimal locking values estimated for each segment, we then varied the location and width of the along-strike transitions to determine where the optimal boundaries that mark the transitions in locking are located, and whether sharp or gradual changes in the locking distribution provide a better fitting model.

In order to locate the boundaries where there are sharp changes in locking distribution, we varied the location of the three potential boundaries indicated by the three node lines in Figure 2a. We varied the location of the first boundary from the first node line in the Kodiak segment to the last node line in the Sanak segment and calculated the residual for each forward model with different locations of the first boundary. The locking distribution in the east side of the boundary is set to be the same as the optimal model in the first segment, and the distribution in the west side of the boundary is the same as the forward model shown in Figure S7. The best location of the first boundary was selected based on the model that has the minimum of the weighted sum of squared residuals (WRSS). After locating the best position of the first boundary, we used the same method to test the best location of the second boundary starting from where the first boundary is located toward the last node line in the west and then do the same for the third boundary.

The optimal locations of the boundaries are shown in Figure 2a. Strong along-strike variation in the estimated locking distribution (Figure 2c) is best described by stepwise decreases in the width of the locked region from the NE to the SW along strike. Besides that, there is a sharp decrease from strongly locked to weakly locked within a short distance in the downdip part of the Kodiak segment, which is different from the more gradual decrease in the locking fraction estimated for the other three segments. However, the strongest locking near the trench cannot be well constrained due to lack of data offshore. Movies S1 to S3 show the data residuals and locking distribution for each forward model when we vary the location of each potential boundary. We also calculated the relative (fractional) increase in residuals above the best fit model and showed the uncertainty range for the location of each boundary based on models that show less than a 20% relative increase in misfit (Figure 2). The locking fraction within the Semidi segment is poorly resolved due to lack of data near the trench (Figures 2 and S5).

We next tested the possibility of gradual along-strike changes in the locking distribution in comparison to the sharp changes in locking assumed in the model of Figure 2a. We varied the width of each boundary tested above and checked how the WRSS changes with the width of the transition. A model with a gradual

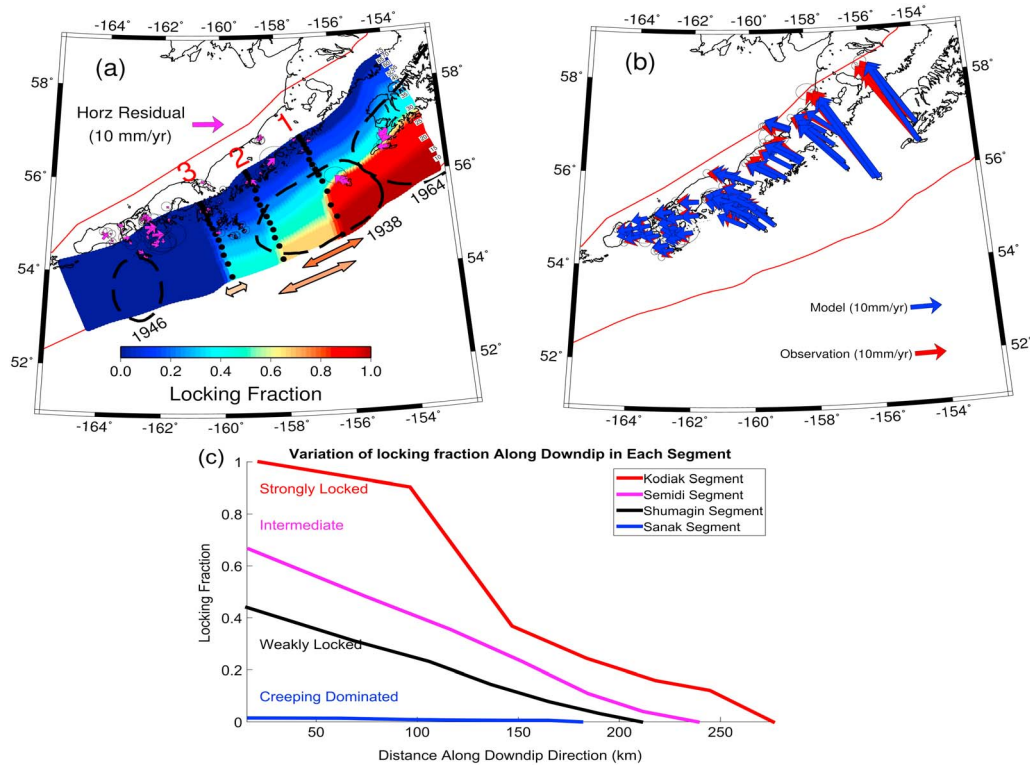


Figure 2. Best fitting model that has the optimal locations of three boundaries mark the sharp changes in locking (a). The orange arrow spans the uncertainty range of the location for the first boundary ($+25$ / -25) km (+ means NE direction and – means SW direction). The yellow-orange arrow spans the uncertainty range of the location for the second boundary ($+150$ / -50) km. The light-orange arrow spans the uncertainty range of the location for the second boundary ($+25$ / -25) km. The observed versus modeled GPS horizontal velocities in the best fitting model (b). Variation of the locking fraction in the downdip direction for each segment from strongly locked to creeping dominated (c).

along-strike change in locking does not provide smaller misfit than the model with abrupt changes, and in most cases, the gradual change produced a worse fit to the data (Movies S4 to S6).

5. Discussion

5.1. Correlation Between the Locking Distribution and the Plate Fabric From Magnetic Anomalies, and Subduction Seismicity

Atwater (1989) examined the magnetic anomaly isochron pattern in the northeast Pacific and its implications for the history of seafloor spreading among the plates within the North Pacific Ocean basin. Her study indicated that the incoming oceanic lithosphere exhibits abrupt changes in seafloor fabric caused by the past seafloor spreading geometry. The pattern of abyssal hills and relic normal faults in the oceanic crust are aligned with the former spreading ridge. Three different preexisting seafloor spreading ridge orientations were identified through the magnetic anomalies: (1) Kula-Pacific spreading from 80 to 56 (44?) Ma at an average rate of ~60 mm/year (Green bold arrow in Figure 3a); (2) Farallon-Pacific spreading from 100 to 55 Ma at a full spreading rate of ~80 mm/year (Magenta bold arrow in Figure 3a); and (3) Vancouver-Pacific spreading from 53 to 30 Ma with the same rate as Farallon-Pacific spreading (Red bold arrow in Figure 3a).

Given the present motion of the Pacific plate, these lateral changes in plate fabric result in abrupt along-strike changes in the fabric of the downgoing plate entering the trench along the Alaska Peninsula. Along-strike variations in preexisting fabric orientations in the Alaska Peninsula strongly correlate with variations in the estimated megathrust locking distribution within the subduction zone. The boundary located between the Kodiak segment and Semidi segment that marks the change from strongly locked to intermediate locked is correlated with the change in preexisting plate fabric due to the cessation of the Kula-Pacific spreading

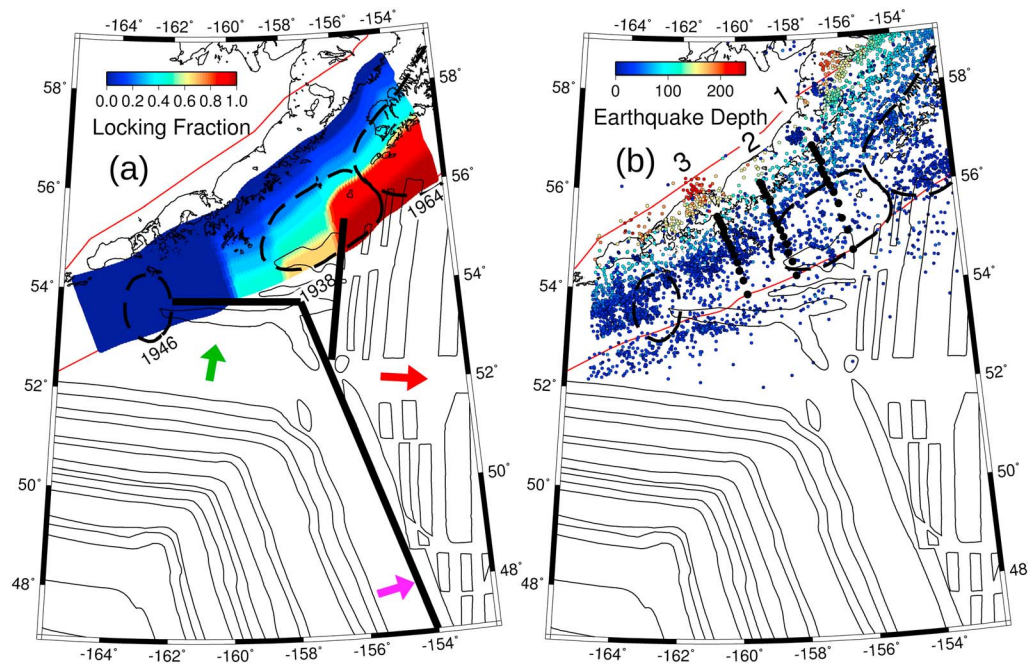


Figure 3. (a) Relationship between significant changes in estimated fault locking and change in preexisting plate fabric based on magnetic anomaly. Digital magnetic anomaly polygons provided by Peter Haeussler and Keith Labay. The original magnetic anomaly data come from Atwater (1989) and Atwater and Severinghaus (1989). Green arrow indicates the spreading direction of the Kula-Pacific spreading center, magenta arrow indicates the spreading direction of the Farallon-Pacific spreading center, and red arrow shows the spreading direction of the Vancouver-Pacific spreading center. The black lines are corresponding to the change in preexisting plate fabric due to the seafloor spreading history based on the magnetic anomalies. (b) Seismicity (Magnitude > 3.0) from the Alaska Earthquake Center from 1990 to present. Numbers 1–3 mark the sharp boundaries of the locking changes.

(intermediate locked) and beginning of the Vancouver-Pacific spreading (strongly locked; Figure 3a). The boundary located between the Semidi segment and the Shumagin segment, which marks the significant change from intermediate to weakly locked, seems to be correlated with the change in preexisting plate fabric where the northern portion of the Farallon plate broke off and became the Vancouver plate with a new spreading direction (Figure 3a). The boundary between the Shumagin segment and the Sanak segment, which marks the change from weakly locked to creeping dominated, is correlated with a major orientation change in two younger sections of preexisting seafloor fabric indicated by the magnetic anomalies near the trench. These correlations suggest that the remnant seafloor structures in the subducting plate are an important control on along-strike variations in megathrust locking distribution within the Alaska Peninsula.

Shillington et al. (2015) proposed that more water is delivered into the subduction zone in the Shumagin segment than in the Semidi segment, where the preexisting downgoing plate fabric is oriented nearly parallel to the trench and promotes bending faulting at the outer rise and that high pore fluid pressure due to hydration affects the intermediate-depth seismicity (van Keken et al., 2011). The correlation between the preexisting fabric orientation and the megathrust slip behavior in our study suggests that more bending faulting and hydration may promote sliding, perhaps through enhanced alternation of clay minerals in the fault zone. Areas where fluids are well drained and remnant fabric is oriented highly oblique ($\geq 90^\circ$) to the trench may experience fluids migrating into and metamorphosing the permeable overlying plate, reducing the pore fluid pressure at the megathrust (Nakajima & Hasegawa, 2016). The decreased pore fluid pressure and fluid leakage increase the effective normal stress with no variation in friction coefficient in a conditionally stable friction regime, which can lead to stick slip behavior and thus a locked megathrust.

Wang and Bilek (2014) summarized that creeping is the dominant mode of subduction when the incoming seafloor is rough and that smooth subducting seafloor results in thrust locking. They pointed out that the Shumagin segment involved subduction of smooth seafloor and was an exception to this rule because it exhibited creep based on previous geodetic observations. However, when the normal faulting at the outer rise is factored in with a relatively thin sediment cover, the seafloor coming into the trench is actually

rougher than for the strongly locked Semidi segment where the faulted basement with a relative thick sediment may result in a relatively smooth contact at depth (Shillington et al., 2015). Therefore, our study area actually agrees well with the relationship between the roughness of seafloor and slip behavior expressed by Wang and Bilek (2014). To sum up, the change in preexisting seafloor fabric structures contributes significantly to the recent locking distribution based on variation in fluid extent and seafloor roughness.

Shallow earthquakes (Figure 3b) are much more common in the regions that are dominated by creep (west of boundary 3) and near the trench in the strongly locked area (east of boundary 1) but are less common in between. Outer-rise earthquakes are more abundant in the creeping-dominated area than the other three areas, and the change in the abundance of outer-rise earthquakes correlates with boundary 3. There are more intermediate-depth earthquakes in the creeping-dominated area (west of boundary 3), fewer in the weakly and intermediate locked areas, and more again in the strongly locked area (east of boundary 1). The spatial pattern of those intermediate-depth earthquakes correlates well with the estimated boundaries in slip behavior within the seismogenic zone in Figures 2 and 3b.

In general, our results suggest that the change in locking distribution is correlated with the change in along-strike subduction seismicity distribution. Shillington et al. (2015) attributed the abundance of outer-rise earthquakes in the creeping segment to the abundant normal faults at the outer rise, and the greater number of intermediate-depth earthquakes to dehydration embrittlement due to high plate hydration. However, intermediate-depth earthquakes are again more abundant in the Kodiak segment, so their argument does not hold for the entire study area. The cause of the correlation pattern between shallow earthquakes and the locking distribution is unclear due to the high uncertainty in locations of those shallow events. For example, we do not know what fraction of those events is due to slip on the plate interface or to faulting in the overriding plate. Our results support the idea that the abundance of normal faults and the resulting hydration of the oceanic plate are both important mechanisms in controlling the locking behavior in comparison with the preexisting plate fabric above. The change in the preexisting seafloor fabric is an important control in variation in megathrust slip and seismicity behavior.

Our model shows distinctive variation in downdip extent of slip deficit along the length of the study area. Our estimated gradual downdip decrease in the locking fraction within the Semidi segment (Figures 2 and 3) can be compared with the identified variations in reflection characteristics of the megathrust fault with depth inferred from seismic reflection by Li et al. (2015). From trench to ~40 km landward, the observed two parallel reflections interpreted as the top and bottom of subducted sediment section correlate well with the region of intermediate locking (~0.7). Then from ~50 to 95 km from the trench, the plate interface appears as a thin reflection band interpreted as a compacted sediment layer matches well with the region of weakly locking (~0.4). Within our region of almost creeping (≤ 0.2), they found a thick reflection band which may be interpreted as a wide deformation zone with branching faults.

Our estimated locking model also shows a correlation with the rupture history of past great earthquakes. The model shows a transition from strongly locked to intermediate locked within the 1938 rupture zone, which is in agreement with the identified two episodes of moment release during this event through waveform modeling, with the second and larger release occurring in the NE part of the rupture zone (Estabrook et al., 1994), which features a wider locked zone. The strongly locked region in the Kodiak segment agrees well with the suggested high moment release under Kodiak Island during 1964 earthquake (Christensen & Beck, 1994).

6. Conclusion

Our model shows three distinct changes in the locking distribution along strike from strongly locked in the Kodiak segment, intermediate in the Semidi segment, and weakly locked in the Shumagin segment, to a creeping-dominated zone in the Sanak segment. The width of the locked region decreases stepwise from NE to SW along strike. We find that the changes in preexisting fabric orientation in the subducting oceanic plate are correlated with the along-strike changes in locking distribution based on variation in fluid extent and seafloor roughness. More outer-rise earthquakes are observed in the creeping-dominated area than in the other three areas. Shallow earthquakes are more common in the creeping-dominated area and near trench in the strongly locked area. More intermediate-depth earthquakes are located downdip of the creeping-dominated and strongly locked areas and fewer in between where the plate fabric is less uniform. The along-strike variations in the subduction seismicity mostly correlate with the changes in the locking

distribution. Our study supports the idea that the preexisting seafloor fabric in the downgoing plate changes the extent of hydration in the oceanic plate along strike and that a strongly hydrated downgoing plate with rough seafloor is more likely to creep, which results in changes in megathrust fault locking distribution and the subduction seismicity.

Acknowledgments

We appreciate Editor Jeroen Ritsema, reviewer Laura Wallace, and Donna Shilington for providing helpful comments that significantly improve the manuscripts. We acknowledge EarthScope for the Plate Boundary Observatory (PBO) data, UNAVCO for operations of the PBO and Alaska Earthquake Center for management of the regional seismic network in Alaska. This research was supported by GeoPRISMS program (NSF award EAR-1457361) to the University of Alaska Fairbanks. We thank Max Kaufman for carrying out the GPS fieldwork in May 2016. We use the Generic Mapping Tools (GMT; Wessel et al., 2013) to draw the figures. The raw data are available in the UNAVCO archive, and our velocities are in the supporting information.

References

- Altamimi, Z., Collilieux, X., & Métivier, L. (2011). ITRF2008: An improved solution of the international terrestrial reference frame. *Journal of Geodesy*, 85(8), 457–473. <https://doi.org/10.1007/s00190-011-0444-4>
- Argus, D. F., Gordon, R. G., Heflin, M. B., Ma, C., Eanes, R. J., Willis, P., et al. (2010). The angular velocities of the plates and the velocity of Earth's centre from space geodesy. *Geophysical Journal International*, 180(3), 913–960. <https://doi.org/10.1111/j.1365-246X.2009.04463.x>
- Atwater, T. (1989). Plate tectonic history of the northeast Pacific and western North America. In E. L. Winterer, D. M. Hussong, & R. W. Decker (Eds.), *The Eastern Pacific Ocean and Hawaii* (v. N, pp. 21–72). Boulder, CO: Geological Society of America, *Geology of North America*.
- Atwater, T., & Severinghaus, J. (1989). Tectonic maps of the northeast Pacific. *The Geology of North America*, 15–20.
- Bécel, A., Shillington, D. J., Delescluse, M., Nedimović, M. R., Abers, G. A., Saffer, D. M., et al. (2017). Tsunamiogenic structures in a creeping section of the Alaska subduction zone. *Nature Geoscience*, 10(8), 609–613. <https://doi.org/10.1038/ngeo2990>
- Christensen, D. H., & Beck, S. L. (1994). The rupture process and tectonic implications of the great 1964 Prince William Sound earthquake. *Pure and Applied Geophysics*, 142(1), 29–53. <https://doi.org/10.1007/BF00875967>
- Cross, R. S., & Freymueller, J. T. (2008). Evidence for and implications of a Bering plate based on geodetic measurements from the Aleutians and western Alaska. *Journal of Geophysical Research*, 113, B07405. <https://doi.org/10.1029/2007JB005136>
- Davies, J., Sykes, L., House, L., & Jacob, K. (1981). Shumagin Seismic Gap, Alaska Peninsula: History of great earthquakes, tectonic setting, and evidence for high seismic potential. *Journal of Geophysical Research*, 86(B5), 3821–3855. <https://doi.org/10.1029/JB086iB05p03821>
- DeGrandpre, K. (2015). Relative sea level change in Western Alaska as constructed from satellite altimetry and repeat GPS measurements (M. Sc. Thesis). University of Alaska Fairbanks.
- Estabrook, C. H., Jacob, K. H., & Sykes, L. R. (1994). Body wave and surface wave analysis of large and great earthquakes along the Eastern Aleutian Arc, 1923–1993: Implications for future events. *Journal of Geophysical Research*, 99, 11,643–11,662. <https://doi.org/10.1029/93JB03124>
- Fletcher, H. J. (2002). Crustal deformation in Alaska measured using the Global Positioning System. University of Alaska Fairbanks.
- Fletcher, H. J., Beavan, J., Freymueller, J., & Gilbert, L. (2001). High interseismic coupling of the Alaska subduction zone SW of Kodiak island inferred from GPS data. *Geophysical Research Letters*, 28, 443–446. <https://doi.org/10.1029/2000GL012258>
- Fournier, T. J., & Freymueller, J. T. (2007). Transition from locked to creeping subduction in the Shumagin region, Alaska. *Geophysical Research Letters*, 34, L06303. <https://doi.org/10.1029/2006GL029073>
- Fournier, T. J., & Freymueller, J. T. (2008). Inflation detected at Mount Veniaminof, Alaska, with campaign GPS. *Geophysical Research Letters*, 35, L20306. <https://doi.org/10.1029/2008GL035503>
- Freymueller, J. T., & Beavan, J. (1999). Absence of strain accumulation in the western Shumagin segment of the Alaska subduction zone. *Geophysical Research Letters*, 26, 3233–3236. <https://doi.org/10.1029/1999GL008356>
- Freymueller, J. T., Woodard, H., Cohen, S. C., Cross, R., Elliott, J., Larsen, C. F., et al. (2008). Active deformation processes in Alaska, based on 15 years of GPS measurements. *Active Tectonics and Seismic Potential of Alaska*, 179, 1–179, 42.
- Hayes, G. P., Wald, D. J., & Johnson, R. L. (2012). Slab1.0: A three-dimensional model of global subduction zone geometries. *Journal of Geophysical Research*, 117, B01302. <https://doi.org/10.1029/2011JB008524>
- Hu, Y., & Freymueller, J. T. (2012). Geodetic observations of Glacial Isostatic Adjustment in Southeast Alaska and its implication of Earth rheology. Abstract Presented at the 2012 G21A-0872 AGU Fall Meeting, San Francisco, CA.
- Johnson, J. M., & Satake, K. (1994). Rupture extent of the 1938 Alaskan earthquake as inferred from tsunami waveforms. *Geophysical Research Letters*, 21, 733–736. <https://doi.org/10.1029/94GL00333>
- Li, J., Shillington, D. J., Bécel, A., Nedimović, M. R., Webb, S. C., Saffer, D. M., et al. (2015). Downdip variations in seismic reflection character: Implications for fault structure and seismogenic behavior in the Alaska subduction zone. *Journal of Geophysical Research: Solid Earth*, 120, 7883–7904. <https://doi.org/10.1002/2015JB012338>
- Li, S., Freymueller, J., & McCaffrey, R. (2016). Slow slip events and time-dependent variations in locking beneath Lower Cook Inlet of the Alaska-Aleutian subduction zone. *Journal of Geophysical Research: Solid Earth*, 121, 1060–1079. <https://doi.org/10.1002/2015JB012491>
- McCaffrey, R. (2002). Crustal block rotations and plate coupling. *Plate boundary zones*. In S. Stein & J. T. Freymueller (Eds.), *Plate boundary zones* (pp. 101–122). Washington, DC: American Geophysical Union. <https://doi.org/10.1029/GD030p0101>
- McCann, W. R., Nishenko, S. P., Sykes, L. R., & Krause, J. (1979). Seismic gaps and plate tectonics: Seismic potential for major boundaries. *Pure and Applied Geophysics*, 117(6), 1082–1147. <https://doi.org/10.1007/BF00876211>
- Nakajima, J., & Hasegawa, A. (2016). Tremor activity inhibited by well-drained conditions above a megathrust. *Nature Communications*, 7, 13863. <https://doi.org/10.1038/ncomms13863>
- Okada, Y. (1985). Surface deformation due to shear and tensile faults in a half-space. *Bulletin of the Seismological Society of America*, 75(4), 1135–1154.
- Sella, G. F., Stein, S., Dixon, T. H., Craymer, M., James, T. S., Mazzotti, S., & Dokka, R. K. (2007). Observation of glacial isostatic adjustment in “stable” North America with GPS. *Geophysical Research Letters*, 34, L02306. <https://doi.org/10.1029/2006GL020781>
- Shillington, D. J., Bécel, A., Nedimović, M. R., Kuehn, H., Webb, S. C., Abers, G. A., et al. (2015). Link between plate fabric, hydration and subduction zone seismicity in Alaska. *Nature Geoscience*, 8(12), 961–964. <https://doi.org/10.1038/ngeo2586>
- Suito, H., & Freymueller, J. T. (2009). A viscoelastic and afterslip postseismic deformation model for the 1964 Alaska earthquake. *Journal of Geophysical Research*, 114, B11404. <https://doi.org/10.1029/2008JB005954>
- van Keken, P. E., Hacker, B. R., Syracuse, E. M., & Abers, G. A. (2011). Subduction factory: 4. Depth-dependent flux of H₂O from subducting slabs worldwide. *Journal of Geophysical Research*, 116, B01401. <https://doi.org/10.1029/2010JB007922>
- Wang, K., & Bilek, S. L. (2014). Invited review paper: Fault creep caused by subduction of rough seafloor relief. *Tectonophysics*, 610, 1–24. <https://doi.org/10.1016/j.tecto.2013.11.024>
- Wessel, P., Smith, W. H., Scharroo, R., Luis, J., & Wobbe, F. (2013). Generic mapping tools: Improved version released. *Eos, Transactions American Geophysical Union*, 94(45), 409–410. <https://doi.org/10.1002/2013EO450001>
- Zou, R., Freymueller, J. T., Ding, K., Yang, S., & Wang, Q. (2014). Evaluating seasonal loading models and their impact on global and regional reference frame alignment. *Journal of Geophysical Research: Solid Earth*, 119, 1337–1358. <https://doi.org/10.1002/2013JB010186>